

Ultrahigh Ionic Exclusion through Carbon Nanomembranes

Yang Yang,* Roland Hillmann, Yubo Qi, Riko Korzetz, Niklas Biere, Daniel Emmrich, Michael Westphal, Björn Büker, Andreas Hütten, André Beyer, Dario Anselmetti, and Armin Götzhäuser*

The collective “single-file” motion of water molecules through natural and artificial nanoconduits inspires the development of high-performance membranes for water separation. However, a material that contains a large number of pores combining rapid water flow with superior ion rejection is still highly desirable. Here, a 1.2 nm thick carbon nanomembrane (CNM) made from cross-linking of terphenylthiol (TPT) self-assembled monolayers is reported to possess these properties. Utilizing their extremely high pore density of 1 sub-nm channel nm⁻², TPT CNMs let water molecules rapidly pass, while the translocation of ions, including protons, is efficiently hindered. Their membrane resistance reaches $\approx 10^4 \Omega \text{ cm}^2$ in 1 M Cl⁻ solutions, comparable to lipid bilayers of a cell membrane. Consequently, a single CNM channel yields an $\approx 10^8$ higher resistance than pores in lipid membrane channels and carbon nanotubes. The ultrahigh ionic exclusion by CNMs is likely dominated by a steric hindrance mechanism, coupled with electrostatic repulsion and entrance effects. The operation of TPT CNM membrane composites in forward osmosis is also demonstrated. These observations highlight the potential of utilizing CNMs for water purification and opens up a simple avenue to creating 2D membranes through molecular self-assembly for highly selective and fast separations.


Osmotic water transport in biological cells is a fundamental process enabling life. To achieve it, nature utilizes aquaporins, membrane proteins with 0.3 nm wide channels that efficiently transport water molecules in a single-file motion across cell membranes but block all ionic species.^[1] This collective movement of water in natural nanoconduits stimulates the development

of artificial membranes to provide clean water for mankind, and the key is to create similarly sized channels.^[2,3] Commercially used osmosis membranes are mostly derived from polymers whose chains are often randomly arranged leading to a broad pore size distribution.^[4] Synthetic nanoconduits like carbon and boron nitride nanotubes,^[5–7] as well as pores made by organic synthesis,^[8] enable a molecular-level control over channel properties and have been demonstrated to provide a fast and efficient water flow through them.^[5,6] However, it remains challenging to produce pores with diameters below 1 nm^[3,9] that can block small ions such as Na⁺, K⁺, and Cl⁻. In addition, the assembly of a large number of channels in parallel into well-defined membranes is a technological challenge.^[3,4] The emergence of 2D materials offers further paths to create such small channels. Recent examples include sub-nm pores made in graphene,^[10,11] and 2D channels assembled between laminae

of graphene oxide^[12] and molybdenum disulfide.^[13] The resulting membranes show a selective ionic permeation, but still lack the pore structures that can prevent all ionic passage. It is therefore highly desirable to develop novel 2D materials with highly ion selective channels that can lay a foundation for advanced osmosis membranes. To address the challenge, it has been proposed utilizing the molecular self-assembly technique assisted with a radiation-induced crosslinking to create one-molecule-thick carbon nanomembranes (CNMs) with defined pore structures.^[14] We have recently reported molecular transport through ≈ 1.2 nm thick CNMs fabricated from terphenylthiol (TPT) monolayers on Au(111) surface.^[15] Low-energy electron exposure of the monolayer induces cleavage of C–H bonds in TPT precursor, and converts the highly ordered molecular structure to a robust, transferable crosslinked carbon network (**Figure 1a**). These nanomembranes permit an extremely high water flow, while being almost impermeable to nonpolar molecules and atoms. This has been attributed to a high areal density ($\approx 10^{18} \text{ m}^{-2}$, i.e., 1 sub-nm pore per square nanometer) of sub-nm channels through which the polar water molecules can pass in a single-file transport.^[15,16] Therewith, the channel density far exceeds $\approx 10^{14}–10^{16} \text{ m}^{-2}$ reached by other nanostructured membranes.^[5,10,17] Hence, these membranes represent a potential new class of 2D membranes toward high-performance

Dr. Y. Yang, Dr. R. Hillmann, Y. Qi, R. Korzetz, N. Biere, D. Emmrich, M. Westphal, B. Büker, Prof. A. Hütten, Dr. A. Beyer, Prof. D. Anselmetti, Prof. A. Götzhäuser
 Faculty of Physics
 Bielefeld University
 33615 Bielefeld, Germany
 E-mail: yang.yang1@imperial.ac.uk; ag@uni-bielefeld.de

Dr. Y. Yang
 Department of Chemical Engineering
 Imperial College London
 London SW7 2AZ, UK

 The ORCID identification number(s) for the author(s) of this article can be found under <https://doi.org/10.1002/adma.201907850>.

© 2020 The Authors. Published by WILEY-VCH Verlag GmbH & Co. KGaA, Weinheim. This is an open access article under the terms of the Creative Commons Attribution License, which permits use, distribution and reproduction in any medium, provided the original work is properly cited.

DOI: 10.1002/adma.201907850

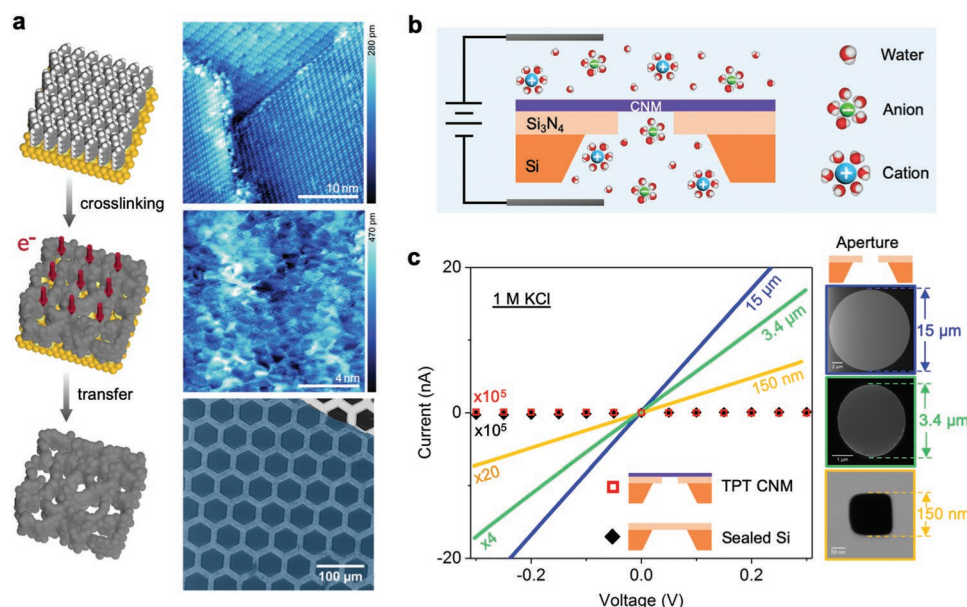


Figure 1. Ion transport measurements with DC method. a) Left panel, schematic illustration of CNM fabrication on Au(111) substrate by electron-induced crosslinking of TPT precursors; right panel, atomic force microscopy images of a self-assembled monolayer (top) and a crosslinked monolayer (i.e., CNM, middle), helium ion microscopy image of a CNM suspended over a hexagonal copper grid (bottom). b) Diagram of ion transport experiments with freestanding TPT CNMs. c) *I*–*V* curves of open apertures (15 μm, 3.4 μm, 150 nm in diameter; the aperture size is determined by helium ion microscope), TPT CNMs suspended over a 15-μm-sized aperture, and a sealed Si₃N₄/Si chip. The measurements were conducted in 1 M KCl solution. Some curves are enhanced by color-coded factors for a better readability. The deviation of measurements between five membrane samples is shown in Figure S3 (Supporting Information).

separations. Further investigation of their permselectivity, especially in liquid mixture systems, will deepen the understanding of the structural and functional properties of such membranes. Here, we will show that the TPT CNMs can block ionic species, including protons, and will also demonstrate the utilization of these materials as very efficient forward osmosis membranes combining high water flux with high ion rejection.

The ion transport was measured by analyzing the current–voltage (*I*–*V*) characteristics of freestanding CNMs mounted on micrometer-sized apertures in Si₃N₄/Si chips (Figure 1b and Figure S1, Supporting Information). This allows a direct measurement of ionic current and eliminates interference from underneath supports. A reference measurement through an open 15 μm aperture in a Si₃N₄/Si chip at 20×10^{-3} M KCl solution shows that after applying 10 mV, a current of 30 nA is detected; the flow is linearly proportional to the applied voltage, fitting well with theoretical predictions (Figure S2, Supporting Information). In 1 M KCl solution, 15 μm, 3.4 μm, and 150 nm sized apertures display resistances of 12 kΩ, 70 kΩ, and 0.8 MΩ, respectively (Figure 1c). In contrast, when the 15 μm sized aperture is covered with a single TPT CNM, the current is indistinguishable from a sealed silicon chip without aperture. TPT CNMs also block ionic currents in other chloride solutions, including HCl, LiCl, NaCl, and MgCl₂. Only very small current fluctuations in a range of –5 to 5 pA at applied voltages from –0.3 to 0.3 V are observed. Some *I*–*V* curves even show a negative slope (Figure S3b, Supporting Information). Taking the fluctuating range as detection limits of the measurements, we can estimate that ions experience a DC resistance of >60 GΩ across TPT CNMs. The reproducibility has been checked with up to five different membrane samples, which all exhibit a

clear ion exclusion behavior. Some small current fluctuations are possibly a consequence of leakage currents, as well as combining effects from electrode reactions and a baseline current drift during measurements.^[18] Similar pA level currents are also detected for sealed silicon chips, constituting a detection limit caused by ion leakage through the sealing of the cell. Helium ion microscopy (HIM) imaging (Figure S4, Supporting Information) and dielectric breakdown experiments (Figure S5, Supporting Information) further indicate that the presence of only few nanometer sized holes in a CNM can lead to fault currents at voltages as low as ≈0.2 V, whereas an intact membrane withstands voltages up to ≈50 V. This confirms that the CNMs were still intact after the measurements, and the observed high ion resistance is a true CNM property and does not arise from an inadequate sample handling or mounting.

In addition, we also performed AC conductivity measurements using electrochemical impedance spectroscopy (EIS) in a frequency range from 10^{–2} to 10⁶ Hz. The corresponding Nyquist plots (Figure 2a,b) were modeled with an equivalent electrical circuit consisting of three components: i) *C*₁, a constant phase element representing a response of membrane capacitance of the nonporous area of CNMs; ii) *R*₁, the ohmic resistance of electrodes, solutions, and electrical contacts that is obtained from the intercepts at the *Z*_{real} axis at high frequency and only amounts to several Ω; iii) *R*₂, the ion transport resistance through CNMs that is determined from the diameter of the semicircle, amounting to several GΩ, which confirms that all ions experience a very high resistance across TPT CNMs. The small differences between the AC and DC resistance values are most likely from deviations between samples and wiring. Compared to the GΩ-level resistances through CNMs,

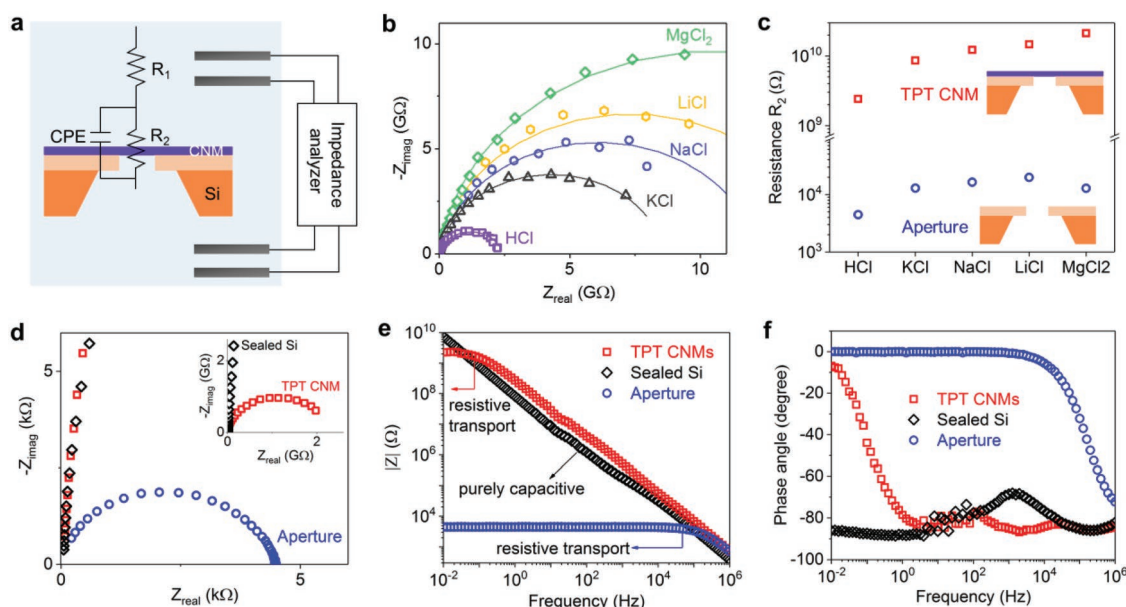


Figure 2. Electrochemical impedance spectra characterization. a) Equivalent circuit model for impedance spectra shown in (b). b) Nyquist plots of impedance spectra for a TPT CNM in 1 M solutions of HCl, LiCl, KCl, NaCl, and MgCl₂. c) Comparison of transport resistance through the aperture and TPT CNM in 1 M chloride solutions. d–f) Nyquist plots, Bode plots of impedance magnitude $|Z|$, and phase shift as a function of frequency for the aperture, TPT CNM, and sealed Si chip in 1 M HCl solution.

an $\approx 10^6$ lower resistance is measured with open apertures of similar size, see Figure 2c, consistent with the DC measurements. It further seems that the few ions translocating through CNMs obey different transport mechanisms with those passing through micrometer-sized apertures. Obviously, the resistance through TPT CNMs relies on the hydration radii of the used cations, in the ascending order of H^+ , K^+ , Na^+ , Li^+ , and Mg^{2+} ; the measurement with MgCl_2 yields the highest resistance despite it contains twice as many anions than the other salts. This implies two membrane properties: First, the limited passage of ions is controlled by an efficient size exclusion mechanism. Second, the membrane can effectively block the penetration of Cl^- ions, which might be related to a negative charged surface originated from the adsorption of anionic species such as hydroxide on the membrane surface.^[19] Figure 2d compares the impedance of a sealed Si chip, a CNM, and an open aperture. One clearly observes the exceedingly high resistance of the CNM even in HCl which has the smallest hydration radius. This is further supported by the associated Bode plots in Figure 2e,f. The sealed chip (black) exhibits a purely capacitive behavior, i.e., while the absolute value of the impedance decreases according to the typical $1/\text{frequency}$ behavior, the phase angle stays nearly constant at -90° . In contrast, the charge flow through CNMs (red) shows a high ($\text{G}\Omega$) resistive transport process in the mHz frequency regime and a capacitive behavior in frequencies larger than a few Hz. The phase angle also shows a gradual shift from 0° to -90° while moving from low to high frequency. An open aperture (blue) presents a similar impedance profile as the TPT CNMs, but with $\approx 10^6$ lower diffusion resistance ($\text{k}\Omega$), the transition from resistive to capacitive occurs at a frequency of $\approx 10^5$ Hz.

To interpret and understand these resistance values, we look into other known systems. Taking the membrane area into

account, the specific resistance for TPT CNMs is calculated to be $\approx 10^4 \Omega \text{ cm}^2$, which is comparable to the high resistances of pure planar lipid bilayers^[20] which have a typical thickness of 3–4 nm. This suggests that the CNM with a thickness of 1.2 nm can repel the penetration of ions like a lipid bilayer does but even at a reduced thickness. The measured CNM resistance is in the same order of magnitude as for lipid bilayers incorporated with a single ion channel.^[21,22] In previous work,^[15] atomic force microscopy (AFM) images revealed a channel density of 10^{18} m^{-2} for TPT CNMs. Combining this with the measured water permeance of $1.13 \times 10^{-4} \text{ mol m}^{-2} \text{ s}^{-1} \text{ Pa}^{-1}$, it was deduced that water molecules travel through a single CNM channel with a similar velocity than through aquaporin and carbon nanotubes (CNTs). In the same way, we also calculate an ion transport resistance of $10^9 \text{ G}\Omega$ for a single CNM channel. This value is impressively high, $\approx 10^8$ times higher than that of other sub-nm channels recorded under similar conditions (Table 1). One way of interpretation is that only very few channels in CNMs are active for mass transport, however, the reduction in the number of effective channels would increase the single-channel water permeation coefficient by the same factor to a value which seems unreasonably high. It is thus more plausible that the CNM channels can extremely suppress the passage of hydrated ions, while water molecules can flow through them.

Our electrochemical data confirm that TPT CNMs can hinder the translocation of ions including protons as the hydration diameter of ions exceeds the effective membrane channel diameter of $\approx 3 \text{ \AA}$.^[15] The passage of few ions detected by EIS could be ascribed to ion leakage or interpreted by a transport in activated regime^[25] where the diffusion relies on bond stretching or flexing. However, we note that the transport of protons in water is commonly illuminated by the Grotthuss mechanism,^[26] where protons can move along the channel by hopping from

Table 1. Ion transport through a single channel at 1 M KCl.

| Channel type | Length | Diameter [nm] | Resistance [$G\Omega$] |
|---|----------------------|-----------------|--------------------------|
| TPT CNMs | ≈ 1.2 nm | ≈ 0.3 | $\approx 10^9$ |
| Natural porin proteins | OmpW ^[21] | ≈ 70 nm | ≈ 0.4 |
| | LamB ^[22] | – | ≈ 0.7 |
| Single-walled CNTs ^[23] | 2 μ m | 0.9 | 0.4 |
| | 5–10 nm | 0.8–1.0 | 5–10 |
| | 5–15 nm | ≈ 1.5 | 1.7 |
| Synthetic channel protein ^[24] | 42 nm | 2 | 1.1 |

one water molecule to another. Accordingly, the rapid water permeation through TPT CNMs should also facilitate the proton transport. Therefore, excepting steric hindrance, other energetic barriers should also contribute to the observed ion exclusion mechanism. It is well known that aquaporin can completely impede the transport of protons.^[1] Simulations provided hints that the water/proton selectivity of aquaporin can be attributed to an electrostatic barrier, but debates remain on whether residual charges^[27] or low dielectric regions^[28] in the protein channel dominate the electrostatic origin. Besides, simulations in CNT systems indicate that protons move very fast along 1D water wires but need to overcome a large energy barrier to enter the channel.^[29] Such an entrance effect might in addition be responsible for the observed proton exclusion in TPT CNMs.

As TPT CNMs possess the desirable combination of high water flux and high ion rejection, we tested their use in forward osmosis (Figure 3). To ensure mechanical stability, cm² sized CNMs were joined with highly porous support structures (Figure S6, Supporting Information). We transferred a single-layer CNM onto a 140 μ m thick polymeric support (3M Microdon) and placed the resulting CNM/Microdon composite with an effective membrane area of ≈ 5 mm² in a permeation cell between a feed solution (FS) of 2×10^{-3} M NaCl and a draw solution (DS) of 1 M NaCl (Figure 3a). However, no significant osmotic water transport was observed, and HIM images revealed that the CNMs had micrometer-sized defects (Figure S6, Supporting Information) that most likely result from the transfer. We sealed these defects by placing a second layer of TPT CNM onto the first one. The water transport properties through freestanding double layer CNMs were measured using the previously used mass-loss permeation experiment,^[15] and we found that water passes these membranes as fast as through a single layer, which can be ascribed to the single-file transport whose flow rate is independent of the channel length.^[30] Through double-layer CNM composites, osmosis then pushes water from the feed side into the draw side (see Video S1, Supporting Information), and within 60 min, the salt concentration in the DS side dropped from 1 to 0.3 M (Figure 3b).

We also joined double-layer CNMs with “track etched” polyethylene terephthalate (TE PET) that possess large (≈ 0.7 μ m) circular pores within a dense PET matrix (Figure S6, Supporting Information). Through these CNM/TE PET composites, osmotic transport is also observed with a flux comparable to CNM/Microdon (Figure 3c). However, as the track-etched pores only make up for $\approx 5\%$ of the total area, the regions of the freestanding CNMs must actually

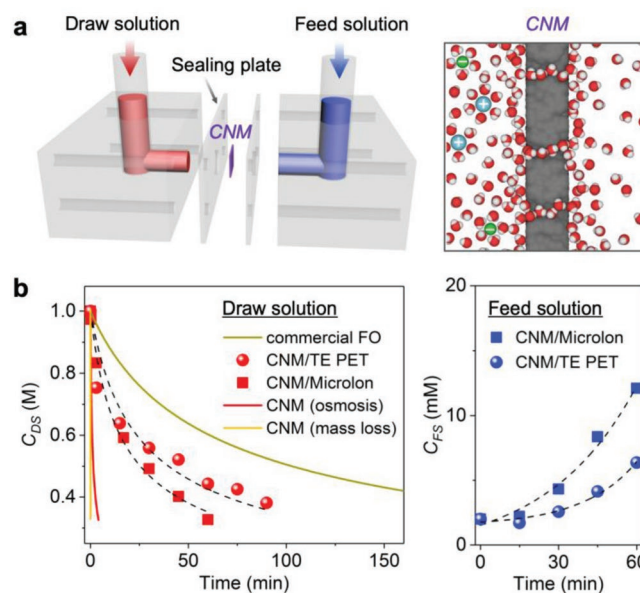


Figure 3. Forward osmosis experiments with double-layer CNMs. a) Left panel, diagram of the permeation cell; right panel, schematic illustration of an effective osmotic process with CNMs: single-file water motion and high ionic exclusion in CNM sub-nm channels. b) Concentration of the draw solution side C_{DS} (1 M NaCl at $t = 0$) and the feed solution side C_{FS} (2×10^{-3} M NaCl at $t = 0$) as a function of time. Plots for CNM/TE PET and CNM/Microdon are made from osmosis experimental data. Plots for commercial FO membrane (HTI-CA) and freestanding CNMs (tested with osmosis and mass-loss experiments) are made from Equation S4 (Supporting Information, see the Experimental Section) using the known water permeance. The black dashed curves in the left panel are fits based on Equation S4 (Supporting Information), and dashed curves in the right panel are exponential fits of the experimental data.

transmit a much faster water flow. From the porosity of TE PET, we extracted a water permeance of ≈ 13 L m⁻² h⁻¹ bar⁻¹ (i.e., 2×10^{-6} mol m⁻² s⁻¹ Pa⁻¹) for freestanding CNMs. This is smaller than the value (≈ 800 L m⁻² h⁻¹ bar⁻¹) determined from the earlier mass-loss measurements,^[15] which is possibly due to the occurrence of internal and external concentration polarization caused by the thick support layer and the unstirred solution in the osmotic process. However, the permeance during osmosis is yet two orders of magnitude higher than for the best known commercial FO membranes (HTI-CA).^[31,32] Assuming an osmotic process under the same conditions, it would only take ≈ 4 min for a freestanding CNM to dilute the DS from 1 to 0.3 M, while the HTI-CA membrane would need ≈ 300 min (Figure 3b). Interestingly, during the osmotic transport, the solute concentration at the FS side only rises from 2 to 6×10^{-3} M for TE PET supported CNM, from which we can extract a reverse flux selectivity (i.e., water flux/salt flux) of ≈ 0.6 m³ mol⁻¹ for freestanding CNMs, which is four times higher than the 0.15 m³ mol⁻¹ achieved by the HTI-CA.^[32] TPT CNMs thus outperform currently used forward osmosis membranes with respect to water flow and ion rejection.

Freestanding TPT CNMs are “ultra-semipermeable” membranes through which water flow occurs up to two orders of magnitude faster than commercial FO membranes. Their high resistance further suggests that the membrane also acts as efficient barriers against ion movement. The advantageous

combination of these membrane properties is mainly attributed to the high density and the small diameters of the sub-nm channels created by the radiation induced cross-linking of TPT molecules. The above results together with the ease of CNM fabrication indicate potential of these membranes for high-performance water separation. Moreover, the CNMs may allow a molecular-level design of membrane properties through a flexible choice of solid substrates and precursor molecules.^[14,33] To put nanofabricated membranes to work, further efforts in large-scale manufacturing as well as a careful embedding of CNM nanoconduits in composites and modules are essential to establish nanotechnology enabled materials separation.

Supporting Information

Supporting Information is available from the Wiley Online Library or from the author.

Acknowledgements

This work was supported by German Federal Ministry of Education and Research (BMBF) under the grants 03X0158A, 02WIL1453B, and 03XP0155A. Y.Y. acknowledges the funding from the European Union's Horizon 2020 research and innovation programme under the Marie Skłodowska-Curie Grant Agreement No. 838593. R.H. and D.A. acknowledge funding from the Deutsche Forschungsgemeinschaft under the grant AN 370/7-1. The authors thank Dr. Nikolaus Meyerbröcker (CNM Technologies GmbH) for providing the track-etched PET support.

Conflict of Interest

The authors declare the following competing financial interest(s): A.G. is a co-founder and shareholder of CNM Technologies GmbH, a company that specializes on the development of carbon nanomembranes. Y.Y. and A.G. are co-authors of a patent for A Method for Separating Fluidic Water from Impure Fluids and a Filter, which is related to the published research.

Keywords

2D materials, nanofluidics, self-assembled monolayer, sub-nanometer channels, water purification

Received: November 29, 2019

Revised: December 19, 2019

Published online: January 16, 2020

- [1] P. Agre, *Angew. Chem., Int. Ed.* **2004**, *43*, 4278.
- [2] K. Gopinadhan, S. Hu, A. Esfandiari, M. Lozada-Hidalgo, F. C. Wang, Q. Yang, A. V. Tyurnina, A. Keerthi, B. Radha, A. K. Geim, *Science* **2019**, *363*, 145.
- [3] J. R. Werber, C. O. Osuji, M. Elimelech, *Nat. Rev. Mater.* **2016**, *1*, 16018.
- [4] H. B. Park, J. Kamcev, L. M. Robeson, M. Elimelech, B. D. Freeman, *Science* **2017**, *356*, eaab0530.
- [5] J. K. Holt, H. G. Park, Y. Wang, M. Stadermann, A. B. Artyukhin, C. P. Grigoropoulos, A. Noy, O. Bakajin, *Science* **2006**, *312*, 1034.
- [6] M. Majumder, N. Chopra, R. Andrews, B. J. Hinds, *Nature* **2005**, *438*, 44.

- [7] A. Siria, P. Poncharal, A. L. Biance, R. Fulcrand, X. Blase, S. T. Purcell, L. Bocquet, *Nature* **2013**, *494*, 455.
- [8] E. Licsandru, I. Kocsis, Y.-X. Shen, S. Murail, Y.-M. Legrand, A. van der Lee, D. Tsai, M. Baaden, M. Kumar, M. Barboiu, *JACS* **2016**, *138*, 5403.
- [9] D. Hedman, H. R. Barzegar, A. Rosén, T. Wågberg, J. A. Larsson, *Sci. Rep.* **2015**, *5*, 16850.
- [10] S. C. O'Hern, M. S. H. Boutilier, J. C. Idrobo, Y. Song, J. Kong, T. Laoui, M. Atieh, R. Karnik, *Nano Lett.* **2014**, *14*, 1234.
- [11] T. Jain, B. C. Raser, R. J. S. Guerrero, M. S. H. Boutilier, S. C. O'Hern, J.-C. Idrobo, R. Karnik, *Nat. Nanotechnol.* **2015**, *10*, 1053.
- [12] a) R. K. Joshi, P. Carbone, F. C. Wang, V. G. Kravets, Y. Su, I. V. Grigorieva, H. A. Wu, A. K. Geim, R. R. Nair, *Science* **2014**, *343*, 752; b) J. Abraham, K. S. Vasu, C. D. Williams, K. Gopinadhan, Y. Su, C. T. Cherian, J. Dix, E. Prestat, S. J. Haigh, I. V. Grigorieva, P. Carbone, A. K. Geim, R. R. Nair, *Nat. Nanotechnol.* **2017**, *12*, 546.
- [13] M. Deng, K. Kwac, M. Li, Y. Jung, H. G. Park, *Nano Lett.* **2017**, *17*, 2342.
- [14] A. Turchanin, A. Götzhäuser, *Adv. Mater.* **2016**, *28*, 6075.
- [15] Y. Yang, P. Dementyev, N. Biere, D. Emmrich, P. Stohmann, R. Korzetz, X. Zhang, A. Beyer, S. Koch, D. Anselmetti, A. Götzhäuser, *ACS Nano* **2018**, *12*, 4695.
- [16] D. Naberezhnyi, A. Götzhäuser, P. Dementyev, *J. Phys. Chem. Lett.* **2019**, *10*, 5598.
- [17] a) K. Celebi, J. Buchheim, R. M. Wyss, A. Droudian, P. Gasser, I. Shorubalko, J. I. J.-I. Kye, C. Lee, H. G. Park, *Science* **2014**, *344*, 289; b) R. L. McGinnis, K. Reimund, J. Ren, L. Xia, M. R. Chowdhury, X. Sun, M. Abril, J. D. Moon, M. M. Merrick, J. Park, K. A. Stevens, J. R. McCutcheon, B. D. Freeman, *Sci. Adv.* **2018**, *4*, e1700938; c) Y. Yang, X. Yang, L. Liang, Y. Gao, H. Cheng, X. Li, M. Zou, R. Ma, Q. Yuan, X. Duan, *Science* **2019**, *364*, 1057.
- [18] R. Penner, in *Single-Channel Recording* (Eds: B. Sakmann, E. Neher), Springer US, Boston, MA **1995**, Ch. 1.
- [19] B. Grosjean, C. Pean, A. Siria, L. Bocquet, R. Vuilleumier, M.-L. Bocquet, *J. Phys. Chem. Lett.* **2016**, *7*, 4695.
- [20] a) S. Micelli, E. Gallucci, D. Meleleo, V. Stipani, V. Picciarelli, *Bioelectrochemistry* **2002**, *57*, 97; b) A. Hirano-Iwata, K. Aoto, A. Oshima, T. Taira, R.-t. Yamaguchi, Y. Kimura, M. Niwano, *Langmuir* **2010**, *26*, 1949; c) M. C. Peterman, J. M. Ziebarth, O. Braha, H. Bayley, H. A. Fishman, D. M. Bloom, *Biomed. Microdevices* **2002**, *4*, 231.
- [21] R. Benz, M. D. Jones, F. Younas, E. Maier, N. Modi, R. Mentele, F. Lottspeich, U. Kleinekathöfer, J. Smit, *PLoS One* **2015**, *10*, e0143557.
- [22] R. Benz, A. Schmid, G. H. Vos-Scheperkeuter, *J. Membr. Biol.* **1987**, *100*, 21.
- [23] a) H. Liu, J. He, J. Tang, H. Liu, P. Pang, D. Cao, P. Krstic, S. Joseph, S. Lindsay, C. Nuckolls, *Science* **2010**, *327*, 64; b) L. Liu, C. Yang, K. Zhao, J. Li, H.-C. Wu, *Nat. Commun.* **2013**, *4*, 2989; c) J. Geng, K. Kim, J. Zhang, A. Escalada, R. Tunuguntla, L. R. Comolli, F. I. Allen, A. V. Shnyrova, K. R. Cho, D. Munoz, Y. M. Wang, C. P. Grigoropoulos, C. M. Ajo-Franklin, V. A. Frolov, A. Noy, *Nature* **2014**, *514*, 612.
- [24] M. Langecker, V. Arnaut, T. G. Martin, J. List, S. Renner, M. Mayer, H. Dietz, F. C. Simmel, *Science* **2012**, *338*, 932.
- [25] L. Wang, M. S. H. Boutilier, P. R. Kidambi, D. Jang, N. G. Hadjiconstantinou, R. Karnik, *Nat. Nanotechnol.* **2017**, *12*, 509.
- [26] C. J. T. Grotthuss, *Ann. Chim.* **1806**, *LVIII*, 54.
- [27] B. L. de Groot, T. Frigato, V. Helms, H. Grubmüller, *J. Mol. Biol.* **2003**, *333*, 279.
- [28] A. Burykin, A. Warshel, *Biophys. J.* **2003**, *85*, 3696.
- [29] C. Dellago, G. Hummer, *Phys. Rev. Lett.* **2006**, *97*, 245901.
- [30] A. Kalra, S. Garde, G. Hummer, *Proc. Natl. Acad. Sci. USA* **2003**, *100*, 10175.
- [31] J. Ren, J. R. McCutcheon, *Desalination* **2014**, *343*, 187.
- [32] S. Lim, M. J. Park, S. Phuntsho, L. D. Tijing, G. M. Nisola, W.-G. Shim, W.-J. Chung, H. K. Shon, *Polymer* **2017**, *110*, 36.
- [33] A. Turchanin, A. Götzhäuser, *Prog. Surf. Sci.* **2012**, *87*, 108.